

A computational method to estimate spin-orbital interaction strength in solid state systems

Qiangqiang Gu^{1,2,*} and Shishir Kumar Pandey^{2,†}

¹*School of Mathematical Science, Peking University, Beijing 100871, China*

²*AI for Science Institute, Beijing, China*

(Dated: November 15, 2022)

Spin-orbit coupling (SOC) drives interesting and non-trivial phenomena in solid state physics, ranging from topological to magnetic to transport properties. Thorough study of such phenomena often require effective models where SOC term is explicitly included. However, estimation of SOC strength for such models mostly depend on the spectroscopy experiments which can only provide a rough estimate. In this work, we provide a simple yet effective computational approach to estimate the on-site SOC strength using a combination of the *ab initio* and tight-binding calculations. We demonstrate the wider applicability and high sensitivity of our method considering materials with varying SOC strengths and the number of SOC active ions. The estimated SOC strengths agree well with the proposed values in literature lending support to our methodology. This simplistic approach can readily be applied to a wide range of materials.

I. INTRODUCTION

The spin-orbit coupling (SOC), a relativistic interaction couples electronic spin (\mathbf{S}) and its orbital momentum (\mathbf{L}) in an atom, causes the splitting of electronic terms into multiplets with total angular momentum $\mathbf{J} = \mathbf{L} + \mathbf{S}$. Dependence of SOC strength λ on atomic number Z as $\sim Z^4$ make this interaction non-perturbative and crucial in heavier elements for accurate description of their electronic structure. When these elements put in a crystal, the situation becomes complex as other splitting terms like crystal field (CF) takes part in determining the electronic structure of a solid. Nevertheless, SOC still manifests its vital role in materials in the form of various interesting physical phenomena. Some of the examples are magnetic anisotropy¹⁻³, spin current⁴, anomalous Hall effect⁵⁻⁸ and the topological properties of materials originating from SOC effects⁹⁻¹⁶. Most recently, in strongly correlated materials, interplay of SOC with other electronic interactions like Coulomb interaction and crystal fields have given rise to exotic phases like unconventional superconductivity¹⁷⁻²⁰ and Kitaev interactions for realization of quantum spin liquid state^{21,22}. Additionally, in 2D materials such as transition metal dichalcogenides (TMDCs), SOC effects can be crucial for possible valleytronic and spintronic applications²³. Given that SOC can strongly modify the electronic structure near the Fermi level resulting in drastic changes in charge carrier mobility and transport properties, its implications in the context of device based applications are also numerous. Thus, SOC effects are imperative for electronic structure modeling of materials in condensed matter physics.

From computation perspective of materials modeling, Density Functional Theory (DFT) based *ab initio* methods have gained wide acceptance for their high transferability and relatively high accuracy. SOC effects can be self-consistently included within this approach. However, in many cases such as strong-correlated materials

or large-scale systems, application of DFT becomes infeasible. A work around in such cases is construction of an effective model e.g. tight-binding (TB), multiband Hubbard-Kanamori²⁴ or Kane-Mele models²⁵, which can closely describe materials properties of interest. Such models have further advantages like their low computation cost, flexibility to explicitly include additional interactions and vary their strengths to examine the corresponding effects on materials properties. As a specific example, one can consider the Hamiltonian $H = H_{\text{TB}} + H_{\text{CF}} + H_{\text{soc}} + H_{\text{int}}$ as an example, where first, second and third terms correspond to CF, SOC and Hubbard-Kanamori interaction terms. This Hamiltonian has been used to estimate the magnetic interactions in so called spin-orbit coupling assisted Mott insulators^{26,27}. One can then vary strength of interactions like λ in the SOC term ($H_{\text{soc}} = \sum_i \lambda_i \mathbf{L}_i \cdot \mathbf{S}_i$, i is atomic index) or intra/inter-orbital Hubbard term (U) and/or Hund's interaction (J_{H}) within H_{int} term²⁷. Techniques such as constrained random-phase-approximation (cRPA) are available to provide estimates of U and J_{H} ²⁸⁻³⁰, while hopping (H_{TB}) and CF terms (H_{CF}) can be estimated from *ab initio* calculation with Wannierization procedure^{26,27,31}.

However, for estimation of λ , one mostly relies on the experiments like low temperature transport spectroscopy, absorption spectroscopy, electoreflectance measurements. Such an estimation of λ , in many cases, may be erroneous. It is because, firstly, spectral features of a solid used to estimate λ may not be solely emerging from SOC effects and more often than not influenced by other structural aspects. This can lead to an "effective" SOC in materials. This is consistent with the fact that in solids with moderate SOC interaction, the atomistic approach to determine strength of SOC cannot be straightforwardly applied. For example, as shown by one of us²⁷ that experimental estimation from SOC assisted excitations brings $\lambda = 15$ meV for Co^{+2} ions in cobaltates and yet our computationally estimated value $\lambda =$

65 meV reproduces experimental features quite well. Secondly, these structural features (e.g. trigonal or tetragonal distortion of an octahedra) may have large variation in different materials. This imply that effective SOC may significantly vary in different materials. However, in the absence of optical measurements for a particular material, one often has to choose value of λ from a broad range available from experiments on other materials belonging to similar class rather than material of interest itself. Given that λ depends on the ionic and spin state of corresponding atom in a solid, such an approach might be amiss or erroneous. Several attempts have been made in the past including some very recent ones to validate and estimate the on-SOC interaction in isolated atoms, monoatomic crystals and binary compounds^{32–35}. However, a general procedure for estimation of λ which can readily be applied to any material of interest is still missing. Computationally, *ab initio* calculations with Wannierization procedure^{31,34} can produce the models that contains the SOC effect. However, in this case, the obtained Wannier orbitals are not necessarily the eigenstates of \hat{S}_z and so, it will be cumbersome to extract λ from such models making their analysis and transferability an issue.

In this paper, we present a simple yet effective method to obtain the strength of SOC for any number of atomic species present in a material. Our method is based on a combination of *ab initio* and Wannier function based tight-binding models (dubbed TBSOC³⁶ hereafter). In this method, we construct a full SOC Hamiltonian defined in the $|\ell_z, s_z\rangle$ basis, which is then used to fit the *ab initio* band structure where the SOC effect is self-consistently introduced. SOC strength is then estimated by fitting the *ab initio* eigenvalues within our model. After introducing the methodology, TBSOC is then tested considering various materials ranging from having weak (3d) to strong (5d) single SOC active ions. We also consider an example of a topological material with two SOC active ions. We show that TBSOC works well on these broad range compounds and the estimated SOC strength is in close agreement with the values found in literature. We also show that the choice of local coordinate system does not affect the result which can further be utilized for additional analysis. These results demonstrate that our TBSOC method offers a direct and convenient way to estimate the strength of SOC in materials.

II. METHODOLOGY

In this section, we first discuss the theoretical background required for implementation of SOC strength followed by methodological procedure discussed next.

A. Theoretical background

The TB Hamiltonian for materials can be described in the form as,

$$H_{\text{TB}} = \sum_{i\alpha, j\beta} T_{i\alpha, j\beta} c_{i\alpha}^\dagger c_{j\beta} + c.c. \quad (1)$$

where the $T_{i\alpha, j\beta}$ are the hopping elements (when $i \neq j$) or onsite element (when $i = j$) between the basis orbitals $|i\alpha\rangle$ and $|j\beta\rangle$. Here i, j are the atomic indices and α, β label the orbitals basis functions. These basis functions can be described in terms of either complex spherical harmonic (Y_ℓ^m) or real/cubic harmonic functions ($X_{\ell m}$) and the two bases are interchangeable using the following unitary transformations.

$$X_{\ell m} = \begin{cases} \frac{i}{\sqrt{2}} \left(Y_\ell^{-|m|} - (-1)^m Y_\ell^{|m|} \right) & m < 0 \\ Y_\ell^0 & m = 0 \\ \frac{1}{\sqrt{2}} \left(Y_\ell^{-|m|} + (-1)^m Y_\ell^{|m|} \right) & m > 0 \end{cases} \quad (2)$$

Above, ℓ is the angular momentum or azimuthal quantum number and m is the magnetic quantum number. However, for efficient computational implementation, the real/cubic harmonic form of orbital basis functions are often considered, functional forms of which are listed in Table. I.

TABLE I. The real/cubic harmonics basis functions $X_{\ell m}$.

| ℓ | $X_{\ell m}$ |
|------------|--|
| $\ell = 0$ | $X_{0,0} = s\rangle = \sqrt{1/4\pi}$ |
| $\ell = 1$ | $X_{1,-1} = p_y\rangle = \sqrt{3/4\pi} \cdot y/r$ $X_{1,0} = p_z\rangle = \sqrt{3/4\pi} \cdot z/r$ $X_{1,1} = p_x\rangle = \sqrt{3/4\pi} \cdot x/r$ |
| $\ell = 2$ | $X_{2,-2} = d_{xy}\rangle = \sqrt{15/4\pi} \cdot xy/r^2$ $X_{2,-1} = d_{yz}\rangle = \sqrt{15/4\pi} \cdot yz/r^2$ $X_{2,0} = d_{z^2}\rangle = \sqrt{5/16\pi} \cdot (3z^2 - r^2)/r^2$ $X_{2,1} = d_{xz}\rangle = \sqrt{15/4\pi} \cdot xz/r^2$ $X_{2,2} = d_{x^2-y^2}\rangle = \sqrt{15/16\pi} \cdot (x^2 - y^2)/r^2$ |

The SOC interaction that couples orbital momentum with that of spin can be accurately approximated by a local “atomic” contribution of form,

$$H_{\text{soc}} = \sum_i \lambda \mathbf{L}_i \cdot \mathbf{S}_i = \lambda \left[\hat{L}_z \hat{S}_z + \frac{1}{2} \left(\hat{L}_+ \hat{S}_- + \hat{L}_- \hat{S}_+ \right) \right] \quad (3)$$

\mathbf{L}_i and \mathbf{S}_i are the angular and spin momentum operator, and \hat{L}_\pm, \hat{S}_\pm are the corresponding raising and lowering operators. Since we are discussing the on-site operators for each site in the crystal, index i is dropped in the right hand side of Eq. 3. The operation of orbital angular momentum operators on the complex spherical harmonics

Y_ℓ^m yields,

$$\begin{aligned} L_\pm Y_\ell^m &= \hbar \sqrt{\ell(\ell+1) - m(m \pm 1)} Y_\ell^{m \pm 1} \\ L_z Y_\ell^m &= \hbar m Y_\ell^m. \end{aligned} \quad (4)$$

The same is also applicable for spin operators.

From Eqs. 2–4, one can obtain the SOC Hamiltonian matrix in the Hilbert subspaces for p and d orbitals considering the basis functions $\alpha/\beta = [p_z, p_x, p_y]$

and $[d_{z^2}, d_{xz}, d_{yz}, d_{x^2-y^2}, d_{xy}]$ respectively. One should note that we haven't considered spin index in the TB Hamiltonian given in Eq. 1 and a full Hamiltonian $\mathcal{H} = H_{\text{TB}} + H_{\text{soc}}$ can be constructed as $\mathcal{H} = \mathcal{I}_2 \otimes H_{\text{TB}} + H_{\text{soc}}$, where \mathcal{I}_2 is the two-dimensional identity matrix and \otimes is the Kronecker product. The complete basis then becomes, $[p_z\uparrow, p_x\uparrow, p_y\uparrow, p_z\downarrow, p_x\downarrow, p_y\downarrow]$ and $[d_{z^2}\uparrow, d_{xz}\uparrow, d_{yz}\uparrow, d_{x^2-y^2}\uparrow, d_{xy}\uparrow, d_{z^2}\downarrow, d_{xz}\downarrow, d_{yz}\downarrow, d_{x^2-y^2}\downarrow, d_{xy}\downarrow]$. Thusly constructed H_{soc} for p and d orbitals are given in Eq. 5 and Eq. 6. Here, λ_p and λ_d are the SOC strength of atomic p and d orbitals.

$$H_{\text{soc}}^p = \frac{\lambda_p}{2} \begin{pmatrix} 0 & 0 & 0 & 0 & -1 & i \\ 0 & 0 & -i & 1 & 0 & 0 \\ 0 & i & 0 & -i & 0 & 0 \\ 0 & 1 & i & 0 & 0 & 0 \\ -1 & 0 & 0 & 0 & 0 & i \\ -i & 0 & 0 & 0 & -i & 0 \end{pmatrix} \quad (5)$$

$$H_{\text{soc}}^d = \frac{\lambda_d}{2} \begin{pmatrix} 0 & 0 & 0 & 0 & 0 & 0 & -\sqrt{3} & i\sqrt{3} & 0 & 0 \\ 0 & 0 & -i & 0 & 0 & \sqrt{3} & 0 & 0 & -1 & i \\ 0 & i & 0 & 0 & 0 & -i\sqrt{3} & 0 & 0 & -i & -1 \\ 0 & 0 & 0 & 0 & -2i & 0 & 1 & i & 0 & 0 \\ 0 & 0 & 0 & 2i & 0 & 0 & -i & 1 & 0 & 0 \\ 0 & \sqrt{3} & i\sqrt{3} & 0 & 0 & 0 & 0 & 0 & 0 & 0 \\ -\sqrt{3} & 0 & 0 & 1 & i & 0 & 0 & i & 0 & 0 \\ -i\sqrt{3} & 0 & 0 & -i & 1 & 0 & -i & 0 & 0 & 0 \\ 0 & -1 & i & 0 & 0 & 0 & 0 & 0 & 0 & 2i \\ 0 & -i & -1 & 0 & 0 & 0 & 0 & 0 & -2i & 0 \end{pmatrix} \quad (6)$$

B. Implementation

Having obtained the H_{SOC} in previously, as the next step, we now describe the complete process for the extraction of SOC strength in solid state materials. The procedure can be divided into mainly three sequential steps given below.

1. Non-spin polarized *ab initio* band structure calculation and its Wannier based TB Hamiltonian (H_{TB}).
2. Self-consistently SOC included *ab initio* band structure calculation.
3. Obtain the optimized SOC strength λ by fitting the band structure of step 2 with Hamiltonian $H_{\text{TB}} + H_{\text{SOC}}$ (of Section II A).

In step 3, the derivatives free Nelder-Mead optimization algorithm^{37,38} is used for error minimization when fitting the *ab initio* eigenvalues to obtain the SOC strength λ .

C. *Ab initio* calculations

In steps 1 and 2 in the previous section, the *ab initio* band structure calculations can be performed with any of the available DFT packages with an interface to Wannier90³⁹. In this paper, we choose Vienna *ab initio* simulation package⁴⁰ for the calculations. Projector-augmented wave method^{41,42} implemented within VASP (version-5.4.4) with the generalized-gradient approximation (GGA) within Perdew-Burke-Ernzerhof framework⁴³ is used and the energy convergence criteria in our self-consistent calculations is when energy difference between successive steps was better than 10^{-5} /unit cell. Details of the plane wave energy cutoff and k -grid used for specific materials is provided in their respective sections.

To summarise our proposed methodology, our TB-SOC program takes in a Wannier function based TB model (H_{TB}) and constructs the full Hamiltonian $\mathcal{H} = H_{\text{TB}} + H_{\text{soc}}$ by adding the on-site H_{soc} term. Starting with a random guess initial value of SOC strength λ , we fit the eigenvalues of SOC included *ab initio* band structure with \mathcal{H} . Error minimization of the fit then leads to

corresponding λ for the atomic species of interest in a material.

III. APPLICATIONS

Having described the methodology in detail, in this section we show the application of TBSOC on some transition metal compounds as well as on a topological material. The transition metal compounds considered here are typical examples for magnetic materials belonging to $3d$, $4d$ and $5d$ class, whose SOC strength ranges from weak to strong. The topological material (TaAs) we consider here is a typical example of non-magnetic and inversion symmetry breaking Weyl semi-metal. The interesting magnetic or topological properties originating from SOC in these materials make them suitable candidates to test our method.

A. The case of transition metal compounds

In this section, as case studies, we demonstrate the estimation of λ in the various transition metal compounds. The choice of materials here is based on three points. First, keeping in mind that SOC strength λ depends on the number of valence electrons (the ionic state of the atom species of interest in a compound). Hence, we choose $\text{Na}_2\text{TeCo}_2\text{O}_6$ ($\text{Co}^{+2}-3d^7$) and $\alpha\text{-RuCl}_3$ ($\text{Ru}^{+3}-4d^5$) as our example systems. Second, given a fixed number of valence electrons, λ changes with atomic number of atomic species of interest. Hence, we show a comparison between iso-electronic $\alpha\text{-RuCl}_3$ ($\text{Ru}^{+3}-4d^5$) and Na_2IrO_3 ($\text{Ir}^{+4}-5d^5$). Third, our choice is also based on the drastic variation of the SOC strength in these materials, which in different cases compete with other interactions like the trigonal/tetragonal crystal field splitting. Magnitude of such splitting in these materials is believed to be in the range 10 – 40 meV⁴⁴ and the SOC strength λ is either comparable or larger than the range of these splitting in the aforementioned compounds. This shows the effectiveness of our methodology apart from its diverse applicability.

As the first example, we showcase the results for $\alpha\text{-RuCl}_3$. For the *ab initio* calculations, we have considered the experimentally observed crystal structure with monoclinic space group $C/2m$ ^{45–47}, crystal structure of which is shown in Fig. 1 (a). We used plane wave energy cutoff 500 eV and Γ -center k -grid of $6 \times 3 \times 6$ in our DFT self-consistent calculations. The layered structure with edge-shared Ru-Cl_6 octahedron are evident from this figure. As described in Section II, in the first step, we construct a TB Hamiltonian (H_{TB}) using Wannier interpolation of the non-spin polarised *ab initio* band structure and the plot is shown in Fig. 1(b). One can see a very good agreement between the two band structures from this figure. This gives us confidence to proceed to the second step in which we calculate the *ab initio* band structure with

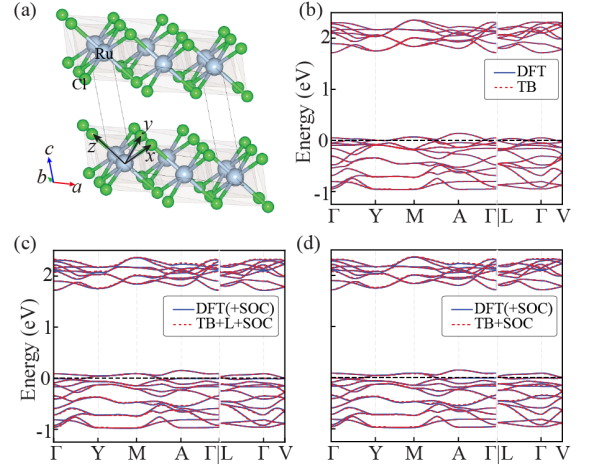


FIG. 1. (a) Crystal structure of $\alpha\text{-RuCl}_3$. Light blue and green balls represent Ru and Cl atoms respectively. a , b and c are the crystallographic axes while x , y and z are the local octahedral coordinate axes. Edge-shared Ru-Cl_6 octahedron are evident. (b) Wannier interpolation of the non-spin polarized *ab initio* band structure of $\alpha\text{-RuCl}_3$ to obtain H_{TB} . All the five d orbitals of Ru are considered in the basis. (c) and (d) show the fitting of SOC included *ab initio* band structure with $H_{\text{TB}} + H_{\text{SOC}}$ in two cases, with and without local octahedral coordinate system respectively. Fermi energy is set to zero.

SOC included at the self-consistent level. We then fit this relativistic band structure with H_{TB} after adding the on-site SOC H_{TB} term. A plot of this fitting procedure is shown in Fig. 1(c). We emphasize here that in both the cases in Fig. 1(b) and (c) we use local octahedral coordinate system shown in Fig. 1(a) to obtain H_{TB} . It is also possible to obtain the estimate of λ is the global crystallographic coordinate axes and fitting procedure is not affected by the choice of coordinate settings. This is evident from Fig. 1(d) where the H_{TB} obtained in global coordinates is used for the fitting. The estimated value of λ in both the cases is ~ 0.120 eV. This value of λ , though in close agreement, is slightly larger by 20 meV from previously experimentally estimated value^{48,49}. As explained in the introduction, underestimation of λ from experiments may come from other structural distortions at play. We emphasize here that further analysis of tight binding model, often required to understand the electronic properties of the material, is not straight forward when global coordinate is used in the honeycomb lattice systems. Hence, we recommend the use of local coordinate system in such cases.

In order to demonstrate the sensitivity of our method, following the same procedure, we estimate λ for two more cases, namely for $\text{Na}_2\text{TeCo}_2\text{O}_6$ and Na_2IrO_3 . For these two cases, strength of SOC varies drastically for Co^{+2} and Ir^{+4} ions. We consider the crystal structure of $\text{Na}_2\text{TeCo}_2\text{O}_6$ with space group $P6_322$ ^{50–55} and Na_2IrO_3 with $C2/m$ ^{56–58} which are shown in Fig. 2(a) and (c) respectively. We used plane wave energy cutoff 550 eV and

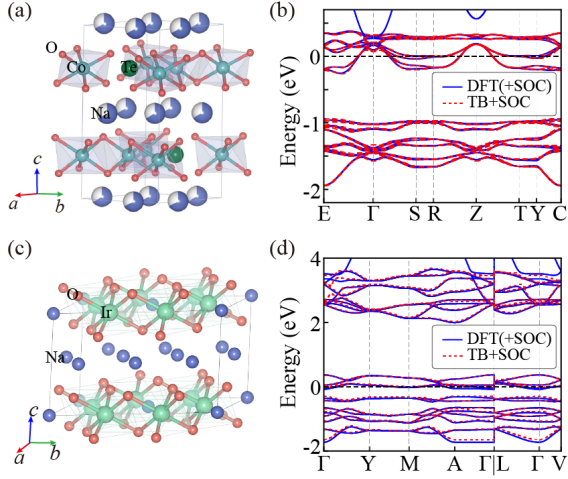


FIG. 2. (a) and (c) Crystal structure of $\text{Na}_3\text{TeCo}_2\text{O}_6$ and Na_2IrO_3 . The white-blue ball in (a) represents partial occupancy of the Na sites. a , b and c are the crystallographic axes. Cyan/green and red balls represent Co/Ir and oxygen atoms respectively. Edge-shared Co/Ir- O_6 octahedron are evident in (a) and (c). (b) and (d) show the fitting of SOC included *ab initio* band structure with a tight binding model after including on-site spin-orbit coupling term for $\text{Na}_3\text{TeCo}_2\text{O}_6$ and Na_2IrO_3 respectively. All the five d orbitals are considered in tight binding basis in both these cases. Fermi energy is set to zero.

Γ -center k -grid of $8 \times 8 \times 4$ for $\text{Na}_3\text{TeCo}_2\text{O}_6$ and $8 \times 6 \times 8$ for Na_2IrO_3 in our DFT self-consistent calculations. Fitting of the SOC included *ab initio* band structure in these two materials is shown in Fig. 2(b) and (d). One can see a very good fitting is obtained in both the cases. Estimated values of λ are 0.065 eV for $\text{Na}_3\text{TeCo}_2\text{O}_6$ and 0.380 eV for Na_2IrO_3 which matches well with the previous experimental estimation⁵⁹.

In this section, we have considered examples in which there were only one spin-orbit coupling activated transition metal ion present. However, there can be more than one atomic species in a material with active spin-orbit coupling interaction. To demonstrated applicability of our method in such cases as well, we consider an example of a topological material, namely TaAs in the next section.

B. The case of topological material

TaAs have been theoretically predicted¹⁵ and then experimentally proved being the topological Weyl semi-metal⁶⁰. Its topological properties such as the surface Fermi arcs¹⁵, edge states⁶¹, surface-bulk connectivity⁶², chiral anomaly⁶³ and non-linear optical responses⁶⁴, etc. have been thoroughly studied and are driven by the SOC effects. In this material, both, the Ta- d and As- p orbitals are considered to be SOC active atoms. It crystallizes in a body-centered-tetragonal structure as shown in Fig. 3(a) with the non-centrosymmetric space group

$I4_1md$. To describe this system, one needs to construct the full Hamiltonian \mathcal{H} as explained earlier. The H_{TB} model in \mathcal{H} is again obtained from non-spin polarised DFT calculation with the Wannier interpolation procedure. The plane wave energy cutoff is set to be 500 eV and Γ -center k -grid of $10 \times 10 \times 4$ are used in the self-consistent DFT calculations. We considered As- p and Ta- d orbitals as the projection basis functions in the TB model. The non-spin polarized *ab initio* band structure and its Wannier interpolation are shown in Fig. 3(b). One can see that the H_{TB} in this case also re-

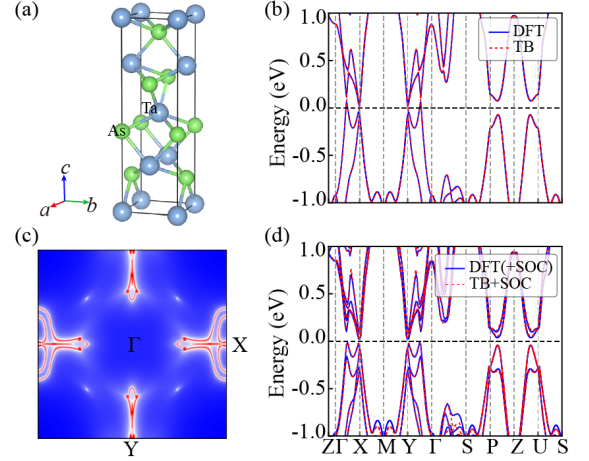


FIG. 3. (a) The body-centered-tetragonal crystals structure of TaAs. Light blue and green balls represent Ta and As atoms respectively. a , b and c are the crystallographic axes. (b) Wannier interpolation of the non-spin polarized *ab initio* band structure of TaAs to obtain H_{TB} . All the five Ta- d and three As- p orbitals are considered in the basis. (c) The (001) surface states calculated using the \mathcal{H} Hamiltonian. (d) Fitting of the SOC included *ab initio* band structure with \mathcal{H} . Fermi energy is set to zero.

produces well the *ab initio* band structure. After adding H_{soc} with parameters λ_p and λ_d to H_{TB} forming \mathcal{H} , we fit the SOC included *ab initio* band structure with \mathcal{H} in the next step. The fit is shown in Fig. 3(d). One can see that the fitting is quite good. This brings $\lambda_p = 0.18$ eV for As- p and $\lambda_d = 0.21$ eV for Ta- d orbitals, which is in the close agreements with the values for Ta atoms as reported in Ref.⁶⁵. For lending support to the reliability of our estimated values of λ 's and thusly obtained full Hamiltonian \mathcal{H} , the (001) As terminated surface states of TaAs is calculated using the iterative Green's function⁶⁶. As shown in Fig. 3(c), a spoon-shaped surface states around the X, and Y points appears on the surface Brillouin zone. Along Γ -X and Γ -Y directions, the Fermi-arc states connect and terminates at the Weyl points, which agrees well with the reported results from literature¹⁵.

IV. CONCLUSION

We have presented a computational framework named TBSOC³⁶ to estimate the strength of SOC in solid state materials. Our methodology is based on the combination of *ab initio* and tight-binding methods. To show its wider applicability, as case studies, we have considered transition metal compounds α -RuCl₃, Na₂TeCo₂O₆ and Na₂IrO₃ and a topological semi-metal TaAs system. We demonstrate the ability of our TBSOC in well reproduc-

ing the self-consistent SOC included *ab initio* band structures. This has been done employing a TB model H_{TB} with addition of on-site SOC term H_{soc} . We show that it works well in both the cases, materials with strong and weak SOC interactions, covering a broad range of materials. We also show that TBSOC works for both local and global coordinate systems, making its utility smoother for further analysis and employment in successive model calculations. This simplistic approach can readily be applied to a wide range of materials.

-
- * guqq@pku.edu.cn
† shishir.kr.pandey@gmail.com
- ¹ B. G. Park, J. Wunderlich, D. A. Williams, S. J. Joo, K. Y. Jung, K. H. Shin, K. Olejník, A. B. Shick, and T. Jungwirth, *Phys. Rev. Lett.* **100**, 087204 (2008).
 - ² D. D. Scherer and B. M. Andersen, *Physical Review Letters* **121**, 037205 (2018).
 - ³ F. Waßer, A. Schneidewind, Y. Sidis, S. Wurmehl, S. Aswartham, B. Büchner, and M. Braden, *Phys. Rev. B* **91**, 060505 (2015).
 - ⁴ J. Sinova, S. O. Valenzuela, J. Wunderlich, C. H. Back, and T. Jungwirth, *Rev. Mod. Phys.* **87**, 1213 (2015).
 - ⁵ A. Vedyayev, N. Ryzhanova, N. Strelkov, and B. Dieny, *Phys. Rev. Lett.* **110**, 247204 (2013).
 - ⁶ M. Y. Zhuravlev, A. Alexandrov, L. Tao, and E. Y. Tsymsal, *Applied Physics Letters* **113**, 172405 (2018).
 - ⁷ A. Matos-Abiad and J. Fabian, *Phys. Rev. Lett.* **115**, 056602 (2015).
 - ⁸ A. Vedyayev, M. Titova, N. Ryzhanova, M. Y. Zhuravlev, and E. Y. Tsymsal, *Applied Physics Letters* **103**, 032406 (2013).
 - ⁹ M. König, S. Wiedmann, C. Brüne, A. Roth, H. Buhmann, L. W. Molenkamp, X.-L. Qi, and S.-C. Zhang, *Science* **318**, 766 (2007).
 - ¹⁰ D. Hsieh, D. Qian, L. Wray, Y. Xia, Y. S. Hor, R. J. Cava, and M. Z. Hasan, *Nature* **452**, 970 (2008).
 - ¹¹ D. Hsieh, Y. Xia, D. Qian, L. Wray, F. Meier, J. Osterwalder, L. Patthey, J. G. Checkelsky, N. Ong, A. V. Fedorov, et al., *Nature* **460**, 1101 (2009).
 - ¹² D. Hsieh, Y. Xia, D. Qian, L. Wray, F. Meier, J. H. Dil, J. Osterwalder, L. Patthey, A. V. Fedorov, H. Lin, A. Bansil, D. Grauer, Y. S. Hor, R. J. Cava, and M. Z. Hasan, *Phys. Rev. Lett.* **103**, 146401 (2009).
 - ¹³ Y. L. Chen, J. G. Analytis, J.-H. Chu, Z. K. Liu, S.-K. Mo, X. L. Qi, H. J. Zhang, D. H. Lu, X. Dai, Z. Fang, S. C. Zhang, I. R. Fisher, Z. Hussain, and Z.-X. Shen, *Science* **325**, 178 (2009).
 - ¹⁴ X. Wan, A. M. Turner, A. Vishwanath, and S. Y. Savrasov, *Phys. Rev. B* **83**, 205101 (2011).
 - ¹⁵ H. Weng, C. Fang, Z. Fang, B. A. Bernevig, and X. Dai, *Phys. Rev. X* **5** (2015).
 - ¹⁶ A. A. Soluyanov, D. Gresch, Z. Wang, Q. Wu, M. Troyer, X. Dai, and B. A. Bernevig, *Nature* **527**, 495 (2015).
 - ¹⁷ B. Kim, H. Ohsumi, T. Komesu, S. Sakai, T. Morita, H. Takagi, and T.-h. Arima, *Science* **323**, 1329 (2009).
 - ¹⁸ Y. Maeno, H. Hashimoto, K. Yoshida, S. Nishizaki, T. Fujita, J. Bednorz, and F. Lichtenberg, *nature* **372**, 532 (1994).
 - ¹⁹ G. Khaliullin, W. Koshibae, and S. Maekawa, *Phys. Rev. Lett.* **93**, 176401 (2004).
 - ²⁰ B. J. Kim, H. Jin, S. J. Moon, J.-Y. Kim, B.-G. Park, C. S. Leem, J. Yu, T. W. Noh, C. Kim, S.-J. Oh, J.-H. Park, V. Durairaj, G. Cao, and E. Rotenberg, *Phys. Rev. Lett.* **101**, 076402 (2008).
 - ²¹ G. Khaliullin, *Progress of Theoretical Physics Supplement* **160**, 155 (2005).
 - ²² G. Jackeli and G. Khaliullin, *Physical review letters* **102**, 017205 (2009).
 - ²³ N. Zibouche, A. Kuc, J. Musfeldt, and T. Heine, *Annalen der Physik* **526**, 395 (2014).
 - ²⁴ A. Georges, L. d. Medici, and J. Mravlje, *Annu. Rev. Condens. Matter Phys.* **4**, 137 (2013).
 - ²⁵ C. L. Kane and E. J. Mele, *Phys. Rev. Lett.* **95**, 226801 (2005).
 - ²⁶ S. K. Pandey, Q. Gu, and R. Tiwari, *arXiv preprint arXiv:2207.05045* (2022).
 - ²⁷ S. K. Pandey and J. Feng, *arXiv preprint arXiv:2205.03836* (2022).
 - ²⁸ S. L. Adler, *Phys. Rev.* **126**, 413 (1962).
 - ²⁹ N. Wiser, *Phys. Rev.* **129**, 62 (1963).
 - ³⁰ F. Aryasetiawan, M. Imada, A. Georges, G. Kotliar, S. Biermann, and A. I. Lichtenstein, *Phys. Rev. B* **70**, 195104 (2004).
 - ³¹ N. Marzari, A. A. Mostofi, J. R. Yates, I. Souza, and D. Vanderbilt, *Reviews of Modern Physics* **84**, 1419 (2012).
 - ³² G. Jha and T. Heine, *Journal of Chemical Theory and Computation* **18**, 4472 (2022), pMID: 35737969.
 - ³³ R. Cuadrado, R. Robles, A. García, M. Pruneda, P. Ordejón, J. Ferrer, and J. I. Cerdá, *Phys. Rev. B* **104**, 195104 (2021).
 - ³⁴ K. Kurita and T. Koretsune, *Phys. Rev. B* **102**, 045109 (2020).
 - ³⁵ M. Vijayakumar and M. Gopinathan, *Journal of Molecular Structure: THEOCHEM* **361**, 15 (1996), theoretical Chemistry in India.
 - ³⁶ Q. Gu, “TBSOC,” <https://github.com/qggu/TBSOC> (2020).
 - ³⁷ J. A. Nelder and R. Mead, *The Computer Journal* **7**, 308 (1965).
 - ³⁸ F. Gao and L. Han, *Computational Optimization and Applications* **51**, 259 (2012).
 - ³⁹ A. A. Mostofi, J. R. Yates, Y.-S. Lee, I. Souza, D. Vanderbilt, and N. Marzari, *Comput. Phys. Commun.* **178**, 685 (2008).
 - ⁴⁰ G. Kresse and J. Furthmüller, *Phys. Rev. B* **54**, 11169 (1996).

- ⁴¹ G. Kresse and D. Joubert, *Phys. Rev. B* **59**, 1758 (1999).
- ⁴² P. E. Blöchl, *Phys. Rev. B* **50**, 17953 (1994).
- ⁴³ J. P. Perdew, K. Burke, and M. Ernzerhof, *Phys. Rev. Lett.* **77**, 3865 (1996).
- ⁴⁴ S. M. Winter, Y. Li, H. O. Jeschke, and R. Valentí, *Phys. Rev. B* **93**, 214431 (2016).
- ⁴⁵ R. D. Johnson, S. C. Williams, A. A. Haghighirad, J. Singleton, V. Zapf, P. Manuel, I. I. Mazin, Y. Li, H. O. Jeschke, R. Valentí, and R. Coldea, *Phys. Rev. B* **92**, 235119 (2015).
- ⁴⁶ H. B. Cao, A. Banerjee, J.-Q. Yan, C. A. Bridges, M. D. Lumsden, D. G. Mandrus, D. A. Tennant, B. C. Chakoumakos, and S. E. Nagler, *Phys. Rev. B* **93**, 134423 (2016).
- ⁴⁷ K. Brodersen, G. Thiele, H. Ohnsorge, I. Recke, and F. Moers, *Journal of the Less Common Metals* **15**, 347 (1968).
- ⁴⁸ K. W. Plumb, J. P. Clancy, L. J. Sandilands, V. V. Shankar, Y. F. Hu, K. S. Burch, H.-Y. Kee, and Y.-J. Kim, *Phys. Rev. B* **90**, 041112 (2014).
- ⁴⁹ L. J. Sandilands, Y. Tian, A. A. Reijnders, H.-S. Kim, K. W. Plumb, Y.-J. Kim, H.-Y. Kee, and K. S. Burch, *Phys. Rev. B* **93**, 075144 (2016).
- ⁵⁰ M. Songvilay, J. Robert, S. Petit, J. A. Rodriguez-Rivera, W. D. Ratcliff, F. Damay, V. Balédent, M. Jiménez-Ruiz, P. Lejay, E. Pachoud, A. Hadj-Azzem, V. Simonet, and C. Stock, *Phys. Rev. B* **102**, 224429 (2020).
- ⁵¹ L. Viciu, Q. Huang, E. Morosan, H. Zandbergen, N. Greenbaum, T. McQueen, and R. Cava, *Journal of Solid State Chemistry* **180**, 1060 (2007).
- ⁵² W. Chen, X. Li, Z. Hu, Z. Hu, L. Yue, R. Sutarto, F. He, K. Iida, K. Kamazawa, W. Yu, X. Lin, and Y. Li, *Phys. Rev. B* **103**, L180404 (2021).
- ⁵³ G. Xiao, Z. Xia, W. Zhang, X. Yue, S. Huang, X. Zhang, F. Yang, Y. Song, M. Wei, H. Deng, *et al.*, *Crystal Growth & Design* **19**, 2658 (2019).
- ⁵⁴ E. Lefrançois, M. Songvilay, J. Robert, G. Nataf, E. Jordan, L. Chaix, C. V. Colin, P. Lejay, A. Hadj-Azzem, R. Ballou, and V. Simonet, *Phys. Rev. B* **94**, 214416 (2016).
- ⁵⁵ A. K. Bera, S. M. Yusuf, A. Kumar, and C. Ritter, *Phys. Rev. B* **95**, 094424 (2017).
- ⁵⁶ Y. Singh, S. Manni, J. Reuther, T. Berlijn, R. Thomale, W. Ku, S. Trebst, and P. Gegenwart, *Phys. Rev. Lett.* **108**, 127203 (2012).
- ⁵⁷ Y. Singh and P. Gegenwart, *Phys. Rev. B* **82**, 064412 (2010).
- ⁵⁸ S. K. Choi, R. Coldea, A. N. Kolmogorov, T. Lancaster, I. I. Mazin, S. J. Blundell, P. G. Radaelli, Y. Singh, P. Gegenwart, K. R. Choi, S.-W. Cheong, P. J. Baker, C. Stock, and J. Taylor, *Phys. Rev. Lett.* **108**, 127204 (2012).
- ⁵⁹ O. F. Schirmer, A. Forster, H. Hesse, M. Wohlecke, and S. Kapphan, *Journal of Physics C: Solid State Physics* **17**, 1321 (1984).
- ⁶⁰ B. Q. Lv, H. M. Weng, B. B. Fu, X. P. Wang, H. Miao, J. Ma, P. Richard, X. C. Huang, L. X. Zhao, G. F. Chen, Z. Fang, X. Dai, T. Qian, and H. Ding, *Phys. Rev. X* **5** (2015).
- ⁶¹ X. Zheng, Q. Gu, Y. Liu, B. Tong, J.-F. Zhang, C. Zhang, S. Jia, J. Feng, and R.-R. Du, *National Science Review* **9**, nwab191 (2022).
- ⁶² H. Inoue, A. Gyenis, Z. Wang, J. Li, S. W. Oh, S. Jiang, N. Ni, B. A. Bernevig, and A. Yazdani, *Science* **351**, 1184 (2016).
- ⁶³ X. Huang, L. Zhao, Y. Long, P. Wang, D. Chen, Z. Yang, H. Liang, M. Xue, H. Weng, Z. Fang, X. Dai, and G. Chen, *Phys. Rev. X* **5**, 031023 (2015).
- ⁶⁴ G. B. Osterhoudt, L. K. Diebel, M. J. Gray, X. Yang, J. Stanco, X. Huang, B. Shen, N. Ni, P. J. W. Moll, Y. Ran, and K. S. Burch, *Nature Materials* **18**, 471 (2019).
- ⁶⁵ K. V. Shanavas, Z. S. Popović, and S. Satpathy, *Phys. Rev. B* **90**, 165108 (2014).
- ⁶⁶ M. P. L. Sancho, J. M. L. Sancho, J. M. L. Sancho, and J. Rubio, *Journal of Physics F: Metal Physics* **15**, 851 (1985).